Biosensors and Bioelectronics 256 (2024) 116277

Contents lists available at ScienceDirect

Biosensors and Bioelectronics

journal homepage: www.elsevier.com/locate/bios

Graphene derivative-based ink advances inkjet printing technology for fabrication of electrochemical sensors and biosensors

Martin-Alex Nalepa [a], David Panáček [a,b], Ivan Dědek [a,c], Petr Jakubec [a], Vojtěch Kupka [a], Vítězslav Hrubý [a,c], Martin Petr [a], Michal Otyepka [a,d,*]

[a] Regional Centre of Advanced Technologies and Materials, Czech Advanced Technology and Research Institute (CATRIN), Palacký University Olomouc, Šlechtitelů 27, Olomouc, 783 71, Czech Republic
[b] Nanotechnology Centre, Centre of Energy and Environmental Technologies, VSB – Technical University of Ostrava, 17. listopadu 2172/15, 708 00, Ostrava-Poruba, Czech Republic
[c] Department of Physical Chemistry, Faculty of Science, Palacký University Olomouc, 17. listopadu 1192/12, Olomouc, 771 46, Czech Republic
[d] IT4Innovations, VSB – Technical University of Ostrava, 17. listopadu 2172/15, Ostrava-Poruba, 708 00, Czech Republic

ARTICLE INFO

Keywords:
Functionalized graphene ink
Inkjet printing
Biosensor
Dopamine detection

ABSTRACT

The field of biosensing would significantly benefit from a disruptive technology enabling flexible manufacturing of uniform electrodes. Inkjet printing holds promise for this, although realizing full electrode manufacturing with this technology remains challenging. We introduce a nitrogen-doped carboxylated graphene ink (NGA-ink) compatible with commercially available printing technologies. The water-based and additive-free NGA-ink was utilized to produce fully inkjet-printed electrodes (IPEs), which demonstrated successful electrochemical detection of the important neurotransmitter dopamine. The cost-effectiveness of NGA-ink combined with a total cost per electrode of $0.10 renders it a practical solution for customized electrode manufacturing. Furthermore, the high carboxyl group content of NGA-ink (13 wt%) presents opportunities for biomolecule immobilization, paving the way for the development of advanced state-of-the-art biosensors. This study highlights the potential of NGA inkjet-printed electrodes in revolutionizing sensor technology, offering an affordable, scalable alternative to conventional electrochemical systems.

1. Introduction

Electrochemical biosensors offer not only high sensitivity and selectivity but also easy implementation, making them well-suited for a diverse set of applications, including point-of-care (PoC) diagnostics (Kim et al., 2019; Wu et al., 2023; Eivazzadeh-Keihan et al., 2022; Soleymani and Li, 2017). These sensors have found widespread use in various established technologies, such as glucose sensing (Heller and Feldman, 2008; Freckmann et al., 2015; Ezzat et al., 2023), lactate detection (Alam et al., 2018; Xuan et al., 2021), cholesterol measurement (Narwal et al., 2019), creatinine analysis (Pundir et al., 2019), and the identification of cancer markers (Jayanthi et al., 2017). The potential of biosensors has also been exploited for detection of coronavirus SARS-COV-19 (Fabiani et al., 2021; Johnston et al., 2022; Vermisoglou et al., 2020; Zhao et al., 2021; Yakoh et al., 2021; Chaibun et al., 2021; Maroli et al., 2023; Rossetti et al., 2024). Biosensing electrodes are typically manufactured through screen-printing technology, which is a cost-effective process suitable for mass production (Suresh et al., 2021). Nevertheless, the screen-printing method requires a peculiar optimization for individual electrode.

New and versatile technologies for manufacturing electrodes are in focus of current research. Inkjet printing emerges as a promising and flexible option that aligns with the principles of Industry 4.0. This is particularly significant considering the need for modularity, i.e., flexible adaptation of factories to changing requirements. Among other printing technologies, inkjet printing excels in handling high value-added inks in small amounts. Moreover, inkjet printing uses dilute inks and deposits them in very small volumes at precise locations, minimizing surface contamination (Lemarchand et al., 2022). The inkjet printing technology operates on a drop-on-demand principle, reducing material waste and providing high-resolution patterning, which can be easily modified via computer software for pattern modifications (Chung et al., 2019;

* Corresponding author. Regional Centre of Advanced Technologies and Materials, Czech Advanced Technology and Research Institute (CATRIN), Palacký University Olomouc, Šlechtitelů 27, Olomouc, 783 71, Czech Republic.
E-mail address: michal.otyepka@upol.cz (M. Otyepka).

https://doi.org/10.1016/j.bios.2024.116277
Received 27 December 2023; Received in revised form 16 March 2024; Accepted 5 April 2024
Available online 7 April 2024

Xuan et al., 2020; Sajedi-Moghaddam et al., 2020). The inkjet printing offers high flexibility, which can be attained by selecting ink with the desired properties or by combining different types of inks.

This concept paves the way for the development of inkjet-printed biosensors, where the inks would contain at least one biological recognition element, such as enzymes, antibodies, nucleic acids, aptamers, or cells (Li et al., 2020; Rosati et al., 2022). Currently, the binding of these biomolecules is limited to gold (Urban et al., 2023) and carbon electrodes, due to the fact that those surfaces can be easily modified by specific functional groups suitable for immobilization of biomolecules (Zub et al., 2022; Silvestri et al., 2023). Graphene, in comparison to gold, combines the benefits of high surface area, unique electrochemical properties, excellent biocompatibility, the possibility to be easily modified by desired functional groups, and last but not least, price.

However, graphene itself does not offer any selectivity and therefore graphene derivatives such as graphene oxide, GO; and reduced graphene oxide, rGO are used as alternatives (Vermisoglou et al., 2020). GO is a nonconductive material and unsuitable for electrochemical readout (Zhao et al., 2023). Conductivity of GO can be reestablished by its reduction to rGO, which may, however, pose another challenges in sensing selectivity due to complex structure of rGO containing various chemical functional groups (Kudr et al., 2020). Very recently graphene derivatives prepared *via* fluorographene chemistry (Chronopoulos et al., 2017) emerged as promising graphene-based materials suitable for sensing. Such water dispersible graphene derivatives are selectively and densely surface-functionalized with chemical moieties, like nitrile, carboxyl, and ethynyl groups (Bakandritsos et al., 2017; Lenarda et al., 2019; Panáček et al., 2021), which have been successfully utilized in sensing (Panáček et al., 2022; Urbanová et al., 2015; Yang et al., 2023) and biosensing applications (Flauzino et al., 2022, 2023). Furthermore, this functionalization creates pathways for the utilization of graphene-derivatives-based inks in nanozyme applications (Hrubý et al., 2022).

The ink used in inkjet printing technology needs to meet several concurrent criteria. These include a particle size compatible with the employed printhead, rheological properties within the range of 1–30 mPa s, surface tension between 30 and 45 mN/m, and appropriate material properties (e.g., dispersion stability and concentration). Several graphene-based inks have already been introduced (Secor et al., 2013; Hersam et al., 2017; Cho et al., 2022; Shao et al., 2020). Graphene ink formulations commonly rely on organic solvents like cyclohexanone and dimethylformamide (Jun et al., 2021) and their use poses health and environmental hazards. In contrast, aqueous systems are sustainable alternatives (Parvez et al., 2019; Pandhi et al., 2020), nevertheless, they are challenged by the difficult dispersion and stabilization of hydrophobic graphene sheets. To overcome this issue, additives are used, however they come with several drawbacks including induction of coffee ring effect, low conductivity, or suppression of biomolecules. It is important to note that inkjet-printed electrodes utilizing water-based graphene inks with desired functional groups have not been implemented on commercial inkjet printers as of yet (Conti et al., 2023; Liu et al., 2023).

In this work, we introduce nitrogen-doped carboxylated-graphene ink (NGA-ink) containing graphene derivative equipped with covalently attached carboxylic groups. The introduced water-based and metal-free NGA-ink contains no additives altering viscosity or surface tension. The NGA-ink contains particles measuring 200–300 nm in lateral size, making it ideally suited for the use with standard commercial inkjet printers. We demonstrate successfully fabricated fully inkjet-printed electrodes, combining commercial silver and gold inks with the NGA-ink. We show that fully inkjet-printed electrodes can be effective in determination of dopamine (DA). Additionally, to delve deeper into the market potential of the fabricated electrodes, we estimated the production cost to be $0.10 per electrode. Considering the above-mentioned benefits, the presented technology opens new horizons for fabrication of wide range of electrochemical biosensors via inkjet printing.

2. Experimental Section

2.1. Inkjet printing process

The printing process was performed using Fujifilm Dimatix Materials Printer, model DMP-2850 equipped with Dimatix Drop Manager v3.2.4.2 software. Samba cartridges featuring piezoelectric printheads with 12 jets and a drop volume of 2.4 pL were used. All patterns were printed in high 2540 dpi resolution, which corresponds to 1.7° head angle and drop spacing of 10 μm. The cartridge temperature was left at the default setting of 28 °C and the platen heating was turned off, keeping the substrate temperature at ambient level. The cartridge print height was set to be 1 mm. Silver nanoparticle ink was shaked for 2 h and filtered sequentially with 1 μm, 450 nm and 200 nm filters with nylon membranes before filling the cartridge. Gold nanoparticle ink was shaked for the same amount of time and filtered two times with 1 μm nylon filter. Polyethylene terephthalate (PET) foil covered with ink-accepting layer was used as a substrate.

Before printing each ink, the jetting waveform and the voltage applied to the jets were optimized to form spherical drops without ligaments or satellite droplets during jetting. Only one jet at a time was used to ensure maximum printing quality. First, the contacts, which are used to connect each electrode with the measuring device through a conductive channel, were printed together with reference electrode using silver nanoparticle ink. Subsequently, counter and working electrode were printed using gold nanoparticle ink. There was a 1.5 mm overlap between silver and gold patterns to ensure a conductive connection between them. After the printing of the gold patterns was finished, the printed parts were allowed to dry completely for half an hour before continuing with the process. In the next step, each printed electrode was flashed once with an external camera flash from a height of 1 cm above the surface. This step was performed to achieve photonic curing of printed metal patterns, causing the sintering of the silver and gold nanoparticles and increasing the conductivity of the printed patterns. Afterwards, NGA-ink was printed onto the working electrode. The dimensions of the pattern were exactly the same as for the gold working electrode beneath. To ensure good coverage of gold surface, 3 layers of NGA-ink were printed over each other. After each layer was printed, there was a 10-min pause to allow the printed ink to dry completely. Four batches of electrodes were printed in total, each containing ~14 individual electrodes.

2.1.1. Post-printing process

After the printing process was completed, liquid silicone rubber was mixed with transparent curing agent and processed as follows. Silicone rubber was thoroughly mixed with curing agent in a weight ratio of 10:1. The mixture was then placed in a vacuum desiccator and degassed for 20 min. Afterwards it was placed into a syringe with a 0.9 mm diameter needle. The resulting mixture was then deposited over the Au/NGA-Ag contact to form a dielectric strip. The complete electrodes were then placed and stored in a vacuum desiccator until the measurement to be sure that all their components are perfectly dry. Prior to electrochemical measurements, the electrodes were cut out in such a shape that they fit into the appropriate adapter.

2.2. Synthesis of NGA-ink

NGA-ink is a <450 nm fraction of nitrogen-doped graphene acid (NGA) material (Fig. 1) synthesized through a two-step batch-type reaction reported recently (Panáček et al., 2022). Briefly, sonicated graphite fluoride reacted with sodium azide in DMF then the product was filtered off and thoroughly washed on the filter. The synthesized nitrogen-doped graphene material (Šedajová et al., 2022) was treated with 45% nitric acid, forming carboxyl functionalities. After successive filtration and washing with water, the prepared NGA material was again strongly sonicated and then dialyzed until the water's conductivity for

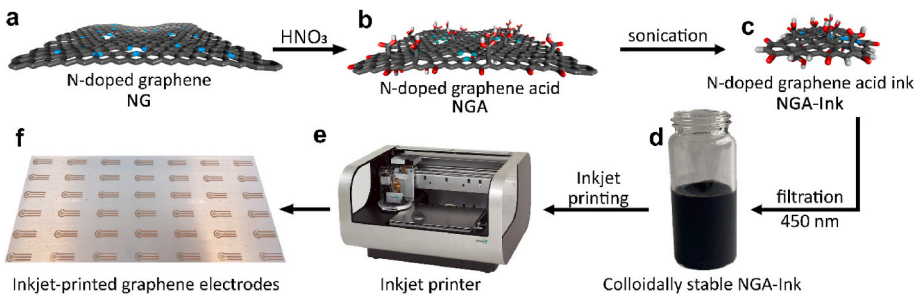

Fig. 1. Synthesis and application of nitrogen-doped graphene acid ink. a) Synthesis of NG precursor (see Ref (Šedajová et al., 2022).), b) oxidation to NGA by nitric acid, and c) downsizing graphene-derivative flakes to NGA-ink with lateral size of 300 nm. d) Image of the highly colloidally stable NGA-ink. e) Dimatix materials printer used for inkjet printing. f) Set of fully inkjet-printed electrodes.

dialysis stopped rising. Finally, after dialyzing, the aqueous NGA dispersion was sonicated for 6 h and then filtered through a 450 nm filter, acquiring NGA-ink dispersion. The pH of the prepared ink was 3.7 due to hydrolysis of the presence of the carboxylic groups on the material. The final concentration of solid component in the NGA-ink was 0.8 mg ml^{-1}. The surface tension of the NGA-ink measured by pendant drop analysis was 59.7 ± 3.2 mN/m (Table S1, Fig. S1), the viscosity at 100 s^{-1} shear rate was 2.4 mPa (Fig. S2). Further experimental details are described in Supporting Information.

3. Results and discussion

3.1. Characterization of NGA-ink

The atomic composition of NGA-ink was probed by X-ray photoelectron spectroscopy (XPS). The freeze-dried NGA-ink was almost fluorine-free (0.9 at. %) carbon material (72.9 at. %) with an oxygen and nitrogen contents of 24.1 at. % and 2.1 at. %, respectively. Deconvolution of the C 1s high-resolution (HR-XPS) spectra region revealed that the most abundant component (58.9 %) was centered at 286.3 eV, representing mainly sp^3 C–C carbons (concerning the elemental composition) and possible C–O and C–N configurations (Fig. 2a). In contrast, the determined sp^2 carbon content was 22.2 %. The high presence of sp^3 carbons arises from the graphene carbons with bonded carboxylic groups. The component around 290.4 eV was, according to its shape and elemental composition, assigned to carboxylic groups (Bakandritsos et al., 2017; Panáček et al., 2022). Feature at 288.2 eV was assigned to lone C═O bonds or possible amide configurations. The presence of C═O and C–O bonds was also evident from the deconvoluted O 1s spectral region (Fig. 2b).

The Infrared spectrum (FT-IR) of the dried NGA-ink (Fig. 2c) exhibited features similar to common organic carboxylic acids, particularly the broad absorption band of O–H stretching between 2700 and 3700 cm^{-1} due to excessive hydrogen bonding of the groups. The absorption bands at 3474 cm^{-1} and 3240 cm^{-1} correspond to various H-bonding configurations. C–H vibrations occur in region between 3200

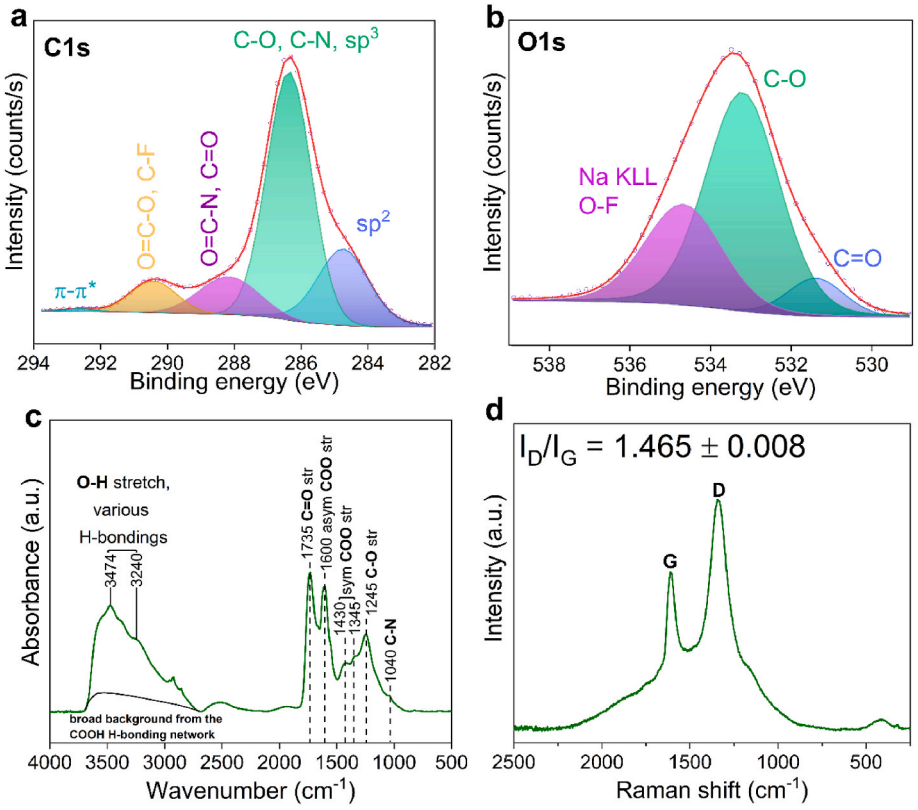

Fig. 2. Deconvoluted HR-XPS spectrum of a) C 1s, and b) O 1s. c) FT-IR spectrum of NGA with assigned vibration bands. d) Raman spectrum of NGA with assigned G and D bands.

and 2800 cm^{-1}. The strongest band of the fingerprint region at 1735 cm^{-1}, typical of C=O stretching, neighbored the second strongest band at 1600 cm^{-1}, assigned to asymmetric stretching of the carboxylic group (Panáček et al., 2022). Symmetric stretching vibration bands at 1430 and 1345 cm^{-1}, as well as C–O stretching at 1245 cm^{-1} (Panáček et al., 2022), lie on a broader feature of skeletal C–C vibrations (Bakandritsos et al., 2017). A shoulder at 1040 cm^{-1} can be assigned to C–N stretching vibrations (Yang et al., 2023). A very high I_D/I_G value of 1.465 determined by Raman spectroscopy as a mean from acquisitions on three different areas on the material (see Fig. 2d with representative data) indicates the highly defective character of the graphene lattice of the NGA-ink caused by high functionalization by carboxyl groups in defects and small lateral size of the graphene flakes (Ferrari et al., 2006; Khan et al., 2010).

3.2. Inkjet printing of NGA-ink

To evaluate its performance and the suitability of NGA-ink for possible electrochemical applications, we have proposed a process for producing inkjet-printed electrodes (Fig. 3a) that is achievable using commercially available inkjet printing technology and further used conventional drop-casting technique and inkjet printing of NGA-ink onto SPCE for comparative reasons. Inkjet printing technology emerges as a superior alternative to conventional drop-casting, offering numerous advantages that are crucial for scientific and industrial applications. The main benefits are the precision of the process and the homogeneity of the resulting coverage of the working electrode. By inkjet printing the material onto the electrode surface, we can reduce adverse effects like the coffee ring effect as well as fouling effect, formation of cracks, and material detachment from the electrode surface during electrochemical experiments (Hanssen et al., 2016; Kaliyaraj Selva Kumar et al., 2020; Sliz et al., 2020). Another strongly undesirable effect is the release of material from the electrode surface into the electrolyte volume during electrochemical measurement when drop-casting is used (Fig. S3). Additionally, inkjet printing stands out in its efficient use of materials, depositing graphene with minimal waste and in several times smaller quantities than drop-casting method. Using this technology, we have investigated the possibility of inkjet printing of 300 nm in lateral size and 3 nm in height graphene flakes (Fig. 3b–e, Fig. S4) onto SPCE and onto fully inkjet-printed electrode. Surfaces of SPCEs and IPEs on PET foil were then analyzed by SEM (Fig. 3f,g,i,j, Fig. S5 a-d). A detailed photograph showing the fully IPE with silver, gold, and NGA-ink parts is shown in Fig. 3h.

The resulting SEM images showed that the surface of the SPCE working electrode is homogeneous and composed purely of carbon particles (Fig. S5 a,b). In contrast, after inkjet printing of the NGA-ink, it is clearly evident that the printing process resulted in uniform functionalization of the SPCE surface with NGA flakes (Fig. S5 c,d). To explore the possibility of using the previously described advantages of inkjet printing technology to produce functionalized electrodes, we engineered fully inkjet-printed electrodes using the process described in detail in the Experimental Section. After inkjet printing of Ag NPs as contacts and reference electrode, we printed Au NPs as counter electrode and working electrode on PET foil (Fig. 3f) substrate. Then, NGA-ink was printed directly onto gold working electrode. SEM images of the IPE showed highly homogeneous surface consisting of Ag (Fig. 3g) and Au (Fig. 3i) NPs of tens of nanometers in size, revealing a remarkable quality of the inkjet-printed electrode. As in previous case with SPCE, after inkjet printing of the NGA-ink onto already printed Au layer, the surface of the gold working electrode was also evenly covered with previously described NGA 300 nm flakes (Fig. 3j). This fact shows that inkjet printing can serve as a tool to functionalize not only a commercially fabricated substrate, but also a surface that is already printed by the same method. In addition, it also demonstrates that complex patterns can be printed using this technology simply by replacing cartridges containing the appropriate inks. Overall, we completely explored the possibilities of modifying electrode surface with the use of inkjet printing and ultimately fabricated fully inkjet-printed electrodes homogeneously functionalized with graphene derivative. To further explore the market viability of the developed electrodes, we conducted a detailed analysis of the production costs of one electrode. Remarkably, the resulting cost of $0.10 per electrode (including all ink and substrate consumption, see Table S2) is exceptionally low, especially considering that the system features a gold working electrode uniformly covered with a functionalized graphene derivative.

The properties of inks are optimized for specific applications through the use of solvents, additives, and binders. Viscosity and surface tension of GO-based ink with water can be adjusted by surface-active compounds such as Triton X-100 and sodium dodecyl sulfate (Li et al., 2018). The use of these surface-active compounds allows for the application of these inks on various substrates, including printing paper and aluminum foil. The majority of described inks utilizes organic solvents such as N-methyl-2-pyrrolidone (Torrisi et al., 2012), dimethylformamide (Lim et al., 2012), and cyclohexanone (Secor et al., 2013, 2015; Gao et al., 2014), along with binders like ethylcellulose (Pandhi et al., 2020) and polyvinylpyrrolidone (Ezzat et al., 2023). In the light of the recent research in this (Table S3), the development of water-based ink not requiring any binder and compatible with marketed inkjet printing technology represents a significant step forward.

3.3. Characterization of electrochemical performance in inkjet-printed electrodes

Electrochemical properties of NGA and its potential for inkjet printing were investigated using electrochemical impedance spectroscopy (EIS). The primary electrochemical characteristics, specifically the charge transfer resistance (R_{CT}), were determined through analysis using modified Randles circuits, as depicted in Fig. 4b. The Nyquist plot in Fig. 4a presents EIS data, highlighting a notable reduction in R_{CT} (more than 10 times) when NGA-ink was applied *via* drop-casting on standard SPCE electrodes. These results suggest NGA-ink's high conductivity. This enhancement can be attributed to NGA's structure. Analysis using XPS and Raman spectroscopy reveals that NGA consists largely of carbon atoms in sp^2 hybridization. Coupled with the material being nitrogen-doped, these observations offer a convincing explanation for the highly conductive properties of this system. The enhancement in conductivity is well demonstrated in the circuit configurations used for interpreting the EIS spectra. Illustrated in Fig. 4b, the circuit design for effectively analyzing the EIS measurements of SPCE electrodes modified with NGA-ink omits the Warburg element, which is usually associated with diffusion-limited processes (Lazanas and Prodromidis, 2023). This implies that using NGA on the electrodes facilitates a more rapid electrochemical reaction compared to the standard, unmodified SPCE electrodes.

3.4. Dopamine sensing using NGA-ink and related inkjet-printed electrode sensor

Conventional cyclic voltammetry and neurotransmitter DA as analyte were selected as the evaluation tool of IPE electrodes. DA can be easily oxidized, leading to the formation of *o*-dopaminechinone *via* a simple two-electron exchange reaction (Dokur et al., 2023; Mounesh et al., 2019; Mounesh and Reddy, 2020). Due to this reason, we have selected NGA-ink because this small-sized graphene-based derivative has favorable properties towards DA determination as proved EIS and *ab initio* calculations. Theoretical computations using range-corrected hybrid density functional with empirical dispersion (ωB97XD) indicated on favorable binding of DA to NGA surface (−130 kcal/mol) in water (Fig. S6 in SI), mostly due to formation of hydrogen bonds and electrostatic interactions. For comparative reasons, we have decided to test commercially available bare SPCE electrodes to provide information about the position of redox peaks as visible in Fig. 5a. As apparent from

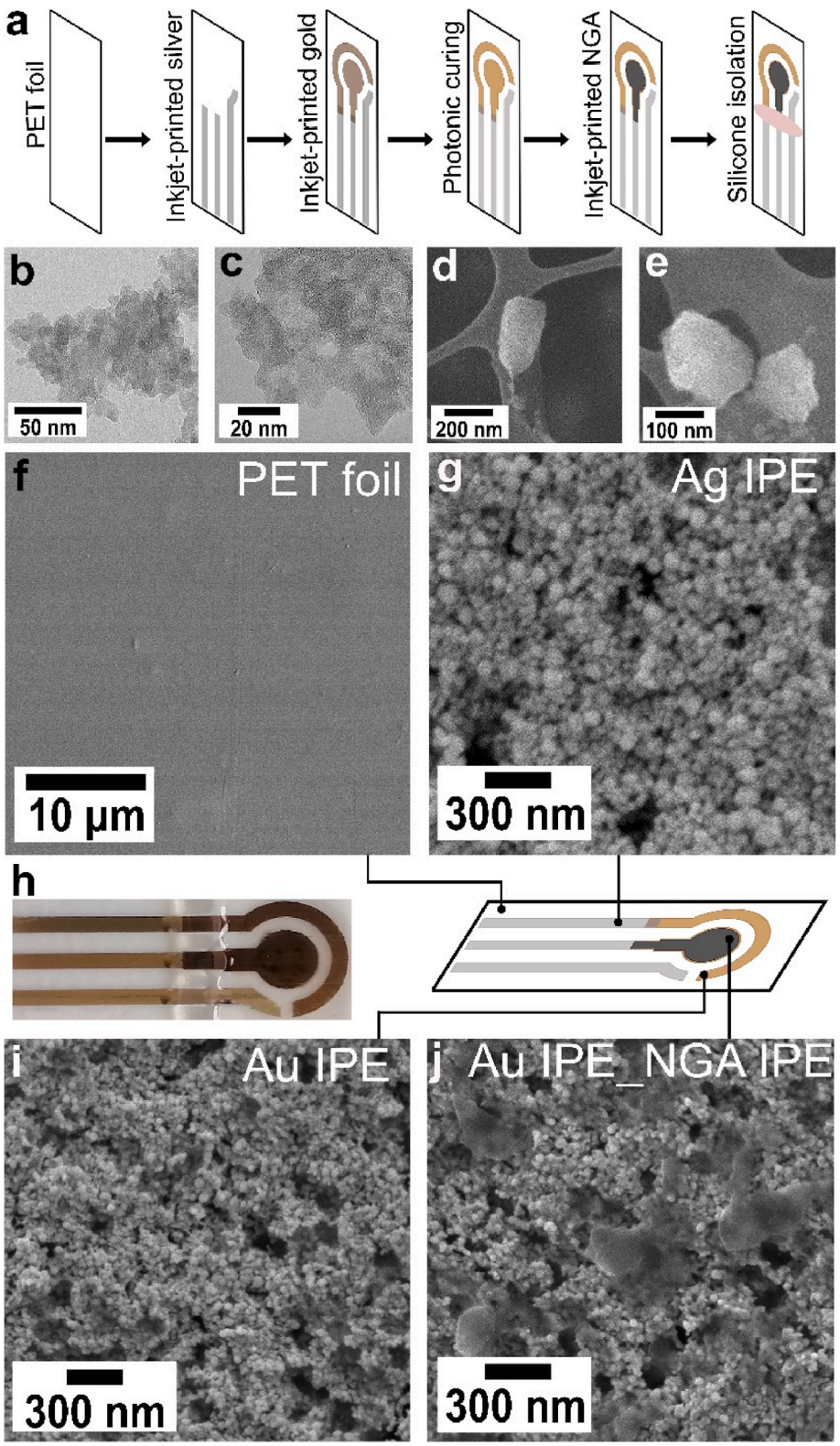

Fig. 3. a) Scheme of the inkjet printing manufacturing process of IPEs, b, c) TEM images of dried NGA-ink, d, e) SEM images of dried NGA-ink indicating lateral size of the flakes in the range of hundreds of nanometers, f) SEM image of PET foil substrate, g) SEM image of inkjet-printed silver pattern, h) A detailed photograph showing the fully IPE i) SEM image of inkjet-printed gold pattern, and j) SEM image of inkjet-printed NGA-ink on inkjet-printed gold substrate with apparent flakes of the carboxylated graphene derivative.

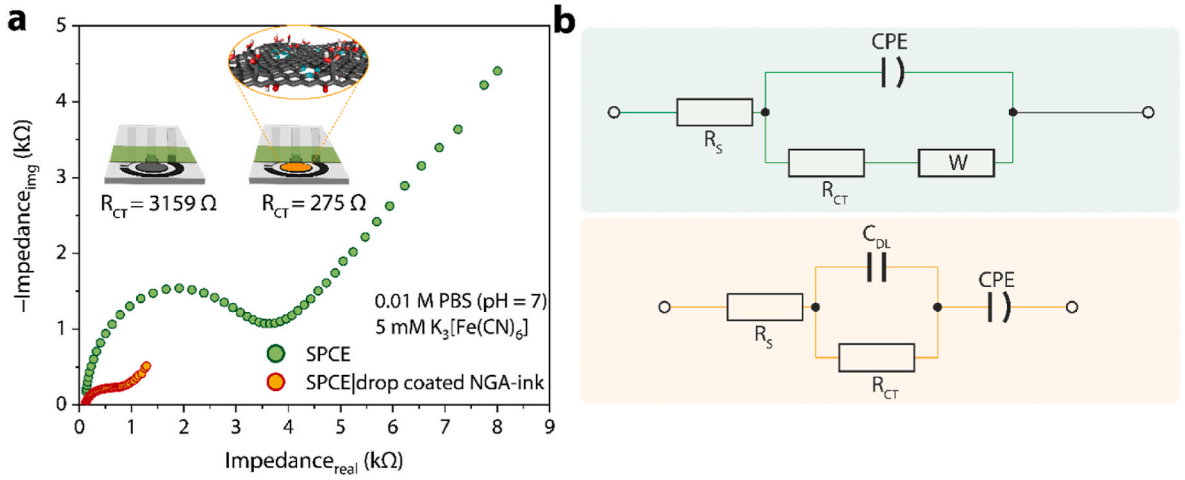

Fig. 4. a) Nyquist plot of bare SPCE electrode (green circles) and SPCE electrode modified with NGA-ink (orange circles) by drop-casting method and b) related modified Randles circuits used for the extraction of R_{CT} value.

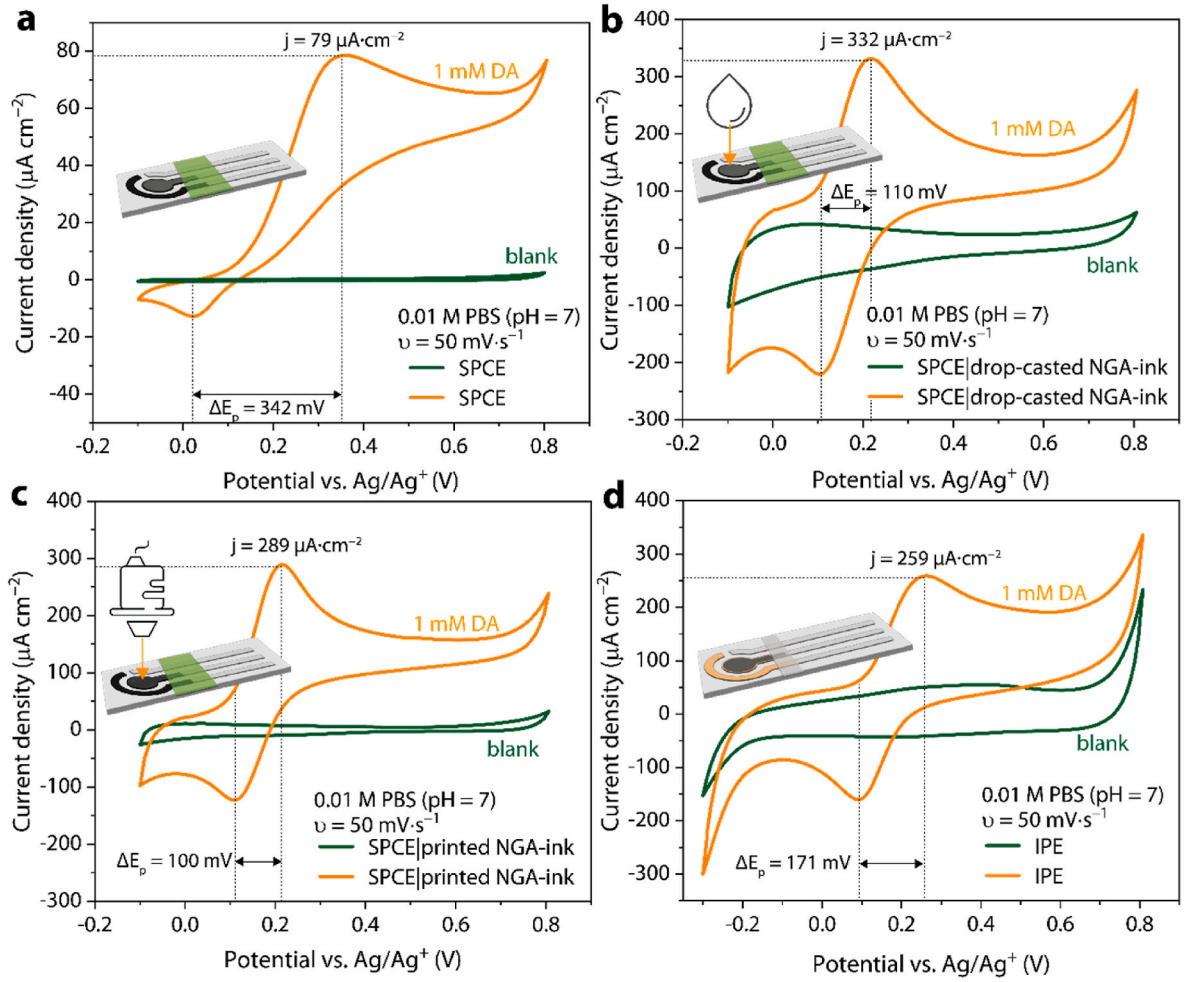

Fig. 5. a) Cyclic voltammograms of bare SPCE electrode in the absence of DA (green line) and in the presence of DA (orange line) and b) similar experiments for NGA-ink drop-casted onto the surface of SPCE working electrode, c) NGA-ink printed *via* inkjet printing technology over the surface of SPCE working electrode at same conditions as previously described and d) CV response of IPE electrode in the absence (green line) and presence (orange line) of DA. All experiments were conducted in 0.01 M PBS buffer (pH = 7) at a scan rate of 50 mV s^{-1}.

results, the value of peak-to-peak separation potential (ΔE_p) is equal to 342 mV. Such result indicates the poor electron transfer kinetics at SPCE electrode probably related to nonconductive components in the commercial ink and because of electrode fouling caused by deposition of DA and its oxidation on the electrode (McCreery, 2008; Ping et al., 2012).

Following the initial stage, NGA-ink was applied via drop-casting onto an SPCE electrode (as shown in Fig. 5b) to improve the electrode kinetics for the determination of DA. In fact, after the formation of NGA film, the current response drastically increased (about 420 %) compared to bare SPCE electrode and value of ΔE_p decreased from 342 mV (pristine SPCE) to ΔE_p: 110 mV indicating faster electrochemical kinetics. Subsequently, the NGA-ink was inkjet-printed *via* Dimatix printer directly onto SPCE working electrode to utilize the aforementioned advantages of inkjet printing over drop-casting method (Fig. 5c). CV response of DA exhibits a well-developed peak of DA giving the current intensity of 289 μA cm^{-2}. There is visible very small current drop compared to drop-casting technique (just 13 % difference) related to the mass of printed material on the surface of the working electrode. In the case of drop-casting technique, the amount of active material equals to 8 μg, while the amount of inkjet-printed active material is equal to 1.2 μg in 5 printed layers. Even with ca 7 times lower amount of active material (NGA-ink), the signal from DA remains well-developed (ΔE_p: 100 mV), indicating suitability of NGA for inkjet printing technology, allowing us to modify the surface of the SPCE electrodes more effectively and more precisely than by drop-casting technique.

Finally, the complete IPE was prepared and tested for DA detection (Fig. 5d). The IPE showed a current response of 259 μA cm^{-2} with ΔE_p at 171 mV, outperforming standard SPCE electrodes. Small drop in sensor activity (ca 10 %) in comparison with NGA-ink printed onto SPCE working electrode is related to application of less conductive substrate in the case of IPE electrode. These results were expected due to the numerous advantages offered by electrodes prepared using inkjet printing technology, as previously discussed, particularly when utilizing small lateral-size graphene flakes. In our specific case, the IPE electrodes benefit from both the uniformity of NGA-ink illustrated as working electrode and the unique properties of NGA-ink, which consists of submicron-sized graphene crystal domains containing numerous point defects within the lattice and closed-contour defects along the edges of the flakes. Therefore, when an electrical bias is applied to the NGA-ink, these defects generate highly localized electric fields that can be influenced by adsorbed molecules or target analytes (Pandhi et al., 2018; Salehi-Khojin et al., 2012). NGA-ink fulfills the requirement for small lateral size sheets, exceptional electrical conductivity, sufficient electroactive surface area (ECSA = 0.088 cm^2; details are provided in SI) and functionalization with carboxylic groups, these characteristics enable the development of highly sensitive graphene-based inkjet-printed sensors, effectively capable of detecting biomolecules like DA.

Additionally, the effectiveness of IPE electrodes was assessed based on their batch-to-batch variability (repeatability) and stability. CV experiments indicate that the variance among four different batches of printed electrodes is approximately 30 %, while the variance among individual electrodes within the same batch is lower, reaching 9 % (Figs. S7a and S7c). The observed variability is caused by an increased capacitive current, as apparent from the CV experiment (Yun and Hwang, 2021), affecting the total current response of the IPE electrodes. This effect is especially visible in the signal changes of electrodes from the 3rd and 4th batches. The differences in capacitive behavior can be explained by variable surface areas related to scratches and inhomogeneities on the electrode surface created during the inkjet printing process and subsequent manipulation of the electrodes (e.g., cutting). Since capacitance is directly proportional to the surface area, an increased surface area leads to increased capacitance (Bakandritsos et al., 2019). To minimize the effect of the capacitive current, specific electrochemical methods, such as pulse techniques that suppress the background current or Electrochemical impedance spectroscopy (EIS), can be utilized in practice. This shows the comparison of IPE electrodes from four batches in Nyquist representation. EIS is a particularly suitable method, primarily due to its sensitivity in detecting both the bulk and interfacial properties of electrodes (Pajkossy and Jurczakowski, 2017; Lazanas and Prodromidis, 2023). This technique can discern variations in electrode composition, structure, and surface chemistry across batches by measuring impedance across a wide frequency range. The EIS response of four series of IPE electrodes (Fig. S7b) provides an almost similar response, indicating low batch-to-batch impedimetric variability of IPE electrodes. Fig. S7c depicts the stability tests of six independent IPE electrodes, proving their stability for at least 14 days without any significant decay. Evaluation of constant concentration of DA at various scan rates revealed that the total surface concentration of DA equals to $\Gamma = 1.07 \times 10^{-7}$ mol cm^{-2} and the heterogenous electron transfer rate constant (k_s) to 2.28 s^{-1} (for details see Fig. S8 and related discussion in SI). Using optimized conditions, IPE electrode was used to determine the different concentrations of DA (Fig. S9) showing a good linear dependence (inset of Fig. S9), and LoD and LoQ values of 46 μM and 140 μM, respectively. These outcomes closely resemble those of a previous experimental setup conducted by (Da Costa et al., 2015), wherein authors employed inkjet-printed carbon nanotubes (CNT) on a paper substrate. Strategies aimed at enhancing the performance of IPE electrodes for sensing may include further optimizing NGA ink conductivity and modification of NGA by conjugation with biomolecules.

4. Conclusion

We introduce water-based, additive-free ink (NGA-ink) containing nitrogen-doped carboxylated graphene (0.8 mg mL^{-1}), compatible with standard inkjet printing technology. We demonstrate that the ink can be used for precise modification of commercial screen-printed carbon electrodes (SPCEs) improving electrode surface homogeneity and reducing material waste with respect to drop-casting method. The fully inkjet-printed electrodes (IPE) are realized using this functional, eco-friendly, and electrochemically active ink. Rigorous testing, including cyclic voltammetry with dopamine (DA) as a proof-of-concept analyte, unravels 9% IPE-to-IPE and 30% batch-to-batch variability in CV response attributed to capacitive behavior. attributed to capacitive behavior. This variability can be significantly mitigated by employing EIS method. Such behavior together with good stability and compatibility of NGA-ink with precision printing technology, and cost-effectiveness pave the way for advanced sensor development. The presence of carboxyl groups in NGA ink offers also covalent attachment to biomolecules like antibodies or aptamers, which can be utilized in construction of fully ink-jet printed biosensors as such offering a significant advancement in sensor technology with its performance, economic, and manufacturing benefits.

CRediT authorship contribution statement

Martin-Alex Nalepa: Writing – original draft, Methodology, Investigation. **David Panáček:** Writing – original draft, Methodology, Investigation, Conceptualization. **Ivan Dědek:** Writing – original draft, Methodology, Investigation. **Petr Jakubec:** Writing – original draft, Visualization, Methodology, Investigation. **Vojtěch Kupka:** Writing – original draft, Methodology, Investigation. **Vítězslav Hrubý:** Writing – original draft, Methodology, Investigation. **Martin Petr:** Investigation. **Michal Otyepka:** Writing – review & editing, Supervision, Funding acquisition, Conceptualization.

Declaration of generative AI and AI-assisted technologies in the writing process

During the preparation of this work the authors used ChatGPT 3.5 and 4.0 for grammar check and assistance in preparation of graphical abstract. After using this tool, the authors carefully reviewed and edited the content as needed and take full responsibility for the content of the publication.

Declaration of competing interest

The authors declare that they have no known competing financial

interests or personal relationships that could have appeared to influence the work reported in this paper.

Data availability

Data are available via ZENODO repository at https://doi.org/10.5281/zenodo.10950733.

Acknowledgements

The work was supported from ERDF/ESF project TECHSCALE (No. CZ.02.01.01/00/22_008/0004587). We also acknowledge financial support of the European Union under the REFRESH – Research Excellence For REgion Sustainability and High-tech Industries (CZ.10.03.01/00/22_003/0000048) via the Operational Programme Just Transition, furthermore the financial support through European Union's Horizon Europe research and innovation programme (project GRADINK nr. 101137959) and the Research Infrastructure NanoEnviCz, supported by the Ministry of Education, Youth and Sports of the Czech Republic under Project No. LM2023066. Ivan Dědek and Vítězslav Hrubý acknowledge the support from the Internal Student Grant Agency of the Palacký University in Olomouc, Czech Republic (IGA_PrF_2024_017). The authors gratefully thank Eirini Ioannou (SEM), Jana Stráská (TEM) and Jiří Hošek (AFM).

Appendix A. Supplementary data

Supplementary data to this article can be found online at https://doi.org/10.1016/j.bios.2024.116277.

References

Alam, F., RoyChoudhury, S., Jalal, A.H., Umasankar, Y., Forouzanfar, S., Akter, N., Bhansali, S., Pala, N., 2018. Lactate biosensing: the emerging point-of-care and personal health monitoring. Biosens. Bioelectron. 117, 818–829. https://doi.org/10.1016/j.bios.2018.06.054.

Bakandritsos, A., Jakubec, P., Pykal, M., Otyepka, M., 2019. Covalently functionalized graphene as a supercapacitor electrode material. FlatChem 13, 25–33. https://doi.org/10.1016/j.flatc.2018.12.004.

Bakandritsos, A., Pykal, M., Błoński, P., Jakubec, P., Chronopoulos, D.D., Poláková, K., Georgakilas, V., Čépe, K., Tomanec, O., Ranc, V., Bourlinos, A.B., Zbořil, R., Otyepka, M., 2017. Cyanographene and graphene acid: emerging derivatives enabling high-yield and selective functionalization of graphene. ACS Nano 11, 2982–2991. https://doi.org/10.1021/acsnano.6b08449.

Chaibun, T., Puenpa, J., Ngamdee, T., Boonapatcharoen, N., Athamanolap, P., O'Mullane, A.P., Vongpunsawad, S., Poovorawan, Y., Lee, S.Y., Lertanantawong, B., 2021. Rapid electrochemical detection of coronavirus SARS-CoV-2. Nat. Commun. 12, 802. https://doi.org/10.1038/s41467-021-21121-7.

Cho, K., Lee, T., Chung, S., 2022. Inkjet printing of two-dimensional van der Waals materials: a new route towards emerging electronic device applications. Nanoscale Horiz 7, 1161–1176. https://doi.org/10.1039/D2NH00162D.

Chronopoulos, D.D., Bakandritsos, A., Pykal, M., Zbořil, R., Otyepka, M., 2017. Chemistry, properties, and applications of fluorographene. Appl. Mater. Today 9, 60–70. https://doi.org/10.1016/j.apmt.2017.05.004.

Chung, S., Cho, K., Lee, T., 2019. Recent progress in inkjet-printed thin-film transistors. Adv. Sci. 6, 1801445 https://doi.org/10.1002/advs.201801445.

Conti, S., Calabrese, G., Parvez, K., Pimpolari, L., Pieri, F., Iannaccone, G., Casiraghi, C., Fiori, G., 2023. Printed transistors made of 2D material-based inks. Nat. Rev. Mater. 8, 651–667. https://doi.org/10.1038/s41578-023-00585-7.

Da Costa, T.H., Song, E., Tortorich, R.P., Choi, J.-W., 2015. A paper-based electrochemical sensor using inkjet-printed carbon nanotube electrodes. ECS J. Solid State Sci. Technol. 4, S3044–S3047. https://doi.org/10.1149/2.0121510jss.

Dokur, E., Uruc, S., Kurteli, R., Gorduk, O., Sahin, Y., 2023. Designing disposable hand-made screen-printed electrode using conductive ink for electrochemical determination of dopamine. Ionics 29, 5465–5480. https://doi.org/10.1007/s11581-023-05239-w.

Eivazzadeh-Keihan, R., Bahojb Noruzi, E., Chidar, E., Jafari, M., Davoodi, F., Kashtiaray, A., Ghafori Gorab, M., Masoud Hashemi, S., Javanshir, S., Ahangari Cohan, R., Maleki, A., Mahdavi, M., 2022. Applications of carbon-based conductive nanomaterials in biosensors. Chem. Eng. J. 442, 136183 https://doi.org/10.1016/j.cej.2022.136183.

Ezzat, M., Rashed, A.E., Sabra, S.A., Haroun, M., El-Moneim, A.A., 2023. Fully inkjet-printed graphene/gold nonenzymatic biosensor for glucose detection. Mater. Today Commun. 37, 107549 https://doi.org/10.1016/j.mtcomm.2023.107549.

Fabiani, L., Saroglia, M., Galatà, G., De Santis, R., Fillo, S., Luca, V., Faggioni, G., D'Amore, N., Regalbuto, E., Salvatori, P., Terova, G., Moscone, D., Lista, F., Arduini, F., 2021. Magnetic beads combined with carbon black-based screen-printed electrodes for COVID-19: a reliable and miniaturized electrochemical immunosensor for SARS-CoV-2 detection in saliva. Biosens. Bioelectron. 171, 112686 https://doi.org/10.1016/j.bios.2020.112686.

Ferrari, A.C., Meyer, J.C., Scardaci, V., Casiraghi, C., Lazzeri, M., Mauri, F., Piscanec, S., Jiang, D., Novoselov, K.S., Roth, S., Geim, A.K., 2006. Raman spectrum of graphene and graphene layers. Phys. Rev. Lett. 97, 187401 https://doi.org/10.1103/PhysRevLett.97.187401.

Flauzino, J.M.R., Nalepa, M., Chronopoulos, D.D., Šedajová, V., Panáček, D., Jakubec, P., Kührová, P., Pykal, M., Banáš, P., Panáček, A., Bakandritsos, A., Otyepka, M., 2023. Click and detect: versatile ampicillin aptasensor enabled by click chemistry on a graphene–alkyne derivative. Small 2207216. https://doi.org/10.1002/smll.202207216.

Flauzino, J.M.R., Nguyen, E.P., Yang, Q., Rosati, G., Panáček, D., Brito-Madurro, A.G., Madurro, J.M., Bakandritsos, A., Otyepka, M., Merkoçi, A., 2022. Label-free and reagentless electrochemical genosensor based on graphene acid for meat adulteration detection. Biosens. Bioelectron. 195, 113628 https://doi.org/10.1016/j.bios.2021.113628.

Freckmann, G., Schmid, C., Baumstark, A., Rutschmann, M., Haug, C., Heinemann, L., 2015. Analytical performance requirements for systems for self-monitoring of blood glucose with focus on system accuracy: relevant differences among ISO 15197:2003, ISO 15197:2013, and current FDA recommendations. J. Diabetes Sci. Technol. 9, 885–894. https://doi.org/10.1177/1932296815580160.

Gao, Y., Shi, W., Wang, W., Leng, Y., Zhao, Y., 2014. Inkjet printing patterns of highly conductive pristine graphene on flexible substrates. Ind. Eng. Chem. Res. 53, 16777–16784. https://doi.org/10.1021/ie502675z.

Hanssen, B.L., Siraj, S., Wong, D.K.Y., 2016. Recent strategies to minimise fouling in electrochemical detection systems. Rev. Anal. Chem. 35, 1–28. https://doi.org/10.1515/revac-2015-0008.

Heller, A., Feldman, B., 2008. Electrochemical glucose sensors and their applications in diabetes management. Chem. Rev. 108, 2482–2505. https://doi.org/10.1021/cr068069y.

Hersam, M.C., Liang, Y.Teng, Secor, E.B., Prabhumirashi, P.L., Puntambekar, K., Geier, M.L., Ahn, B., Lewis, J., 2017. Methods for preparation of concentrated graphene ink compositions and related composite materials. WO/2017/035193. WO/2017/035193.

Hrubý, V., Zaoralová, D., Medveď, M., Bakandritsos, A., Zbořil, R., Otyepka, M., 2022. Emerging graphene derivatives as active 2D coordination platforms for single-atom catalysts. Nanoscale 14, 13490–13499. https://doi.org/10.1039/D2NR03453K.

Jayanthi, V.S.P., Das, A.B., Saxena, U., 2017. Recent advances in biosensor development for the detection of cancer biomarkers. Biosens. Bioelectron. 91, 15–23. https://doi.org/10.1016/j.bios.2016.12.014.

Johnston, M., Ceren Ates, H., Glatz, R.T., Mohsenin, H., Schmachtenberg, R., Göppert, N., Huzly, D., Urban, G.A., Weber, W., Dincer, C., 2022. Multiplexed biosensor for point-of-care COVID-19 monitoring: CRISPR-powered unamplified RNA diagnostics and protein-based therapeutic drug management. Mater. Today 61, 129–138. https://doi.org/10.1016/j.mattod.2022.11.001.

Jun, H.-Y., Kim, S.-J., Choi, C.-H., 2021. Ink formulation and printing parameters for inkjet printing of two dimensional materials: a mini review. Nanomaterials 11, 3441. https://doi.org/10.3390/nano11123441.

Kaliyaraj Selva Kumar, A., Zhang, Y., Li, D., Compton, R.G., 2020. A mini-review: how reliable is the drop casting technique? Electrochem. Commun. 121, 106867 https://doi.org/10.1016/j.elecom.2020.106867.

Khan, U., O'Neill, A., Lotya, M., De, S., Coleman, J.N., 2010. High-concentration solvent exfoliation of graphene. Small 6, 864–871. https://doi.org/10.1002/smll.200902066.

Kim, J., Campbell, A.S., De Ávila, B.E.-F., Wang, J., 2019. Wearable biosensors for healthcare monitoring. Nat. Biotechnol. 37, 389–406. https://doi.org/10.1038/s41587-019-0045-y.

Kudr, J., Zhao, L., Nguyen, E.P., Arola, H., Nevanen, T.K., Adam, V., Zitka, O., Merkoçi, A., 2020. Inkjet-printed electrochemically reduced graphene oxide microelectrode as a platform for HT-2 mycotoxin immunoenzymatic biosensing. Biosens. Bioelectron. 156, 112109 https://doi.org/10.1016/j.bios.2020.112109.

Lazanas, A.Ch, Prodromidis, M.I., 2023. Electrochemical impedance Spectroscopy—A tutorial. ACS Meas. Sci. Au 3, 162–193. https://doi.org/10.1021/acsmeasuresciau.2c00070.

Lemarchand, J., Bridonneau, N., Battaglini, N., Carn, F., Mattana, G., Piro, B., Zrig, S., Noël, V., 2022. Challenges, prospects, and emerging applications of inkjet-printed electronics: a chemist's point of view. Angew. Chem. Int. Ed. 61, e202200166 https://doi.org/10.1002/anie.202200166.

Lenarda, A., Bakandritsos, A., Bevilacqua, M., Tavagnacco, C., Melchionna, M., Naldoni, A., Steklý, T., Otyepka, M., Zbořil, R., Fornasiero, P., 2019. Selective functionalization blended with scaffold conductivity in graphene acid promotes H_2O_2 electrochemical sensing. ACS Omega 4, 19944–19952. https://doi.org/10.1021/acsomega.9b02881.

Li, P., Tao, C.-A., Wang, B., Huang, J., Li, T., Wang, J., 2018. Preparation of graphene oxide-based ink for inkjet printing. J. Nanosci. Nanotechnol. 18, 713–718. https://doi.org/10.1166/jnn.2018.13942.

Li, X., Liu, B., Pei, B., Chen, J., Zhou, D., Peng, J., Zhang, X., Jia, W., Xu, T., 2020. Inkjet bioprinting of biomaterials. Chem. Rev. 120, 10793–10833. https://doi.org/10.1021/acs.chemrev.0c00008.

Lim, S., Kang, B., Kwak, D., Lee, W.H., Lim, J.A., Cho, K., 2012. Inkjet-printed reduced graphene oxide/poly(vinyl alcohol) composite electrodes for flexible transparent organic field-effect transistors. J. Phys. Chem. C 116, 7520–7525. https://doi.org/10.1021/jp203441e.

Liu, Y., Zhu, H., Xing, L., Bu, Q., Ren, D., Sun, B., 2023. Recent advances in inkjet-printing technologies for flexible/wearable electronics. Nanoscale 15, 6025–6051. https://doi.org/10.1039/D2NR05649F.

Maroli, G., Abarintos, V., Piper, A., Merkoçi, A., 2023. The cleanroom-free, cheap, and rapid fabrication of nanoelectrodes with low zM limits of detection. Small 19, 2302136. https://doi.org/10.1002/smll.202302136.

McCreery, R.L., 2008. Advanced carbon electrode materials for molecular electrochemistry. Chem. Rev. 108, 2646–2687. https://doi.org/10.1021/cr068076m.

Mounesh, Malathesh, P., Praveen Kumara, N.Y., Jilani, B.S., Mruthyunjayachari, C.D., Venugopala Reddy, K.R., 2019. Synthesis and characterization of tetra-ganciclovir cobalt (II) phthalocyanine for electroanalytical applications of AA/DA/UA. Heliyon 5, e01946. https://doi.org/10.1016/j.heliyon.2019.e01946.

Mounesh, Reddy, K.R.V., 2020. Novel garnished cobalt(ii) phthalocyanine with MWCNTs on modified GCE: sensitive and reliable electrochemical investigation of paracetamol and dopamine. New J. Chem. 44, 16831–16844. https://doi.org/10.1039/D0NJ03926H.

Narwal, V., Deswal, R., Batra, B., Kalra, V., Hooda, R., Sharma, M., Rana, J.S., 2019. Cholesterol biosensors: a review. Steroids 143, 6–17. https://doi.org/10.1016/j.steroids.2018.12.003.

Pajkossy, T., Jurczakowski, R., 2017. Electrochemical impedance spectroscopy in interfacial studies. Curr. Opin. Electrochem. 1, 53–58. https://doi.org/10.1016/j.coelec.2017.01.006.

Panáček, D., Hochvaldová, L., Bakandritsos, A., Malina, T., Langer, M., Belza, J., Martincová, J., Večeřová, R., Lazar, P., Poláková, K., Kolařík, J., Válková, L., Kolář, M., Otyepka, M., Panáček, A., Zbořil, R., 2021. Silver covalently bound to cyanographene overcomes bacterial resistance to silver nanoparticles and antibiotics. Adv. Sci. 8, 2003090 https://doi.org/10.1002/advs.202003090.

Panáček, D., Zdražil, L., Langer, M., Šedajová, V., Baďura, Z., Zoppellaro, G., Yang, Q., Nguyen, E.P., Álvarez-Diduk, R., Hrubý, V., Kolařík, J., Chalmpes, N., Bourlinos, A. B., Zbořil, R., Merkoçi, A., Bakandritsos, A., Otyepka, M., 2022. Graphene nanobeacons with high-affinity pockets for combined, selective, and effective decontamination and reagentless detection of heavy metals. Small 18, 2201003. https://doi.org/10.1002/smll.202201003.

Pandhi, T., Cornwell, C., Fujimoto, K., Barnes, P., Cox, J., Xiong, H., Davis, P.H., Subbaraman, H., Koehne, J.E., Estrada, D., 2020. Fully inkjet-printed multilayered graphene-based flexible electrodes for repeatable electrochemical response. RSC Adv. 10, 38205–38219. https://doi.org/10.1039/D0RA04786D.

Pandhi, T., Kreit, E., Aga, R., Fujimoto, K., Sharbati, M.T., Khademi, S., Chang, A.N., Xiong, F., Koehne, J., Heckman, E.M., Estrada, D., 2018. Electrical transport and power dissipation in aerosol-jet-printed graphene interconnects. Sci. Rep. 8, 10842 https://doi.org/10.1038/s41598-018-29195-y.

Parvez, K., Worsley, R., Alieva, A., Felten, A., Casiraghi, C., 2019. Water-based and inkjet printable inks made by electrochemically exfoliated graphene. Carbon 149, 213–221. https://doi.org/10.1016/j.carbon.2019.04.047.

Ping, J., Wu, J., Wang, Y., Ying, Y., 2012. Simultaneous determination of ascorbic acid, dopamine and uric acid using high-performance screen-printed graphene electrode. Biosens. Bioelectron. 34, 70–76. https://doi.org/10.1016/j.bios.2012.01.016.

Pundir, C.S., Kumar, P., Jaiwal, R., 2019. Biosensing methods for determination of creatinine: a review. Biosens. Bioelectron. 126, 707–724. https://doi.org/10.1016/j.bios.2018.11.031.

Rosati, G., Urban, M., Zhao, L., Yang, Q., De Carvalho Castro E Silva, C., Bonaldo, S., Parolo, C., Nguyen, E.P., Ortega, G., Fornasiero, P., Paccagnella, A., Merkoçi, A., 2022. A plug, print & play inkjet printing and impedance-based biosensing technology operating through a smartphone for clinical diagnostics. Biosens. Bioelectron. 196, 113737 https://doi.org/10.1016/j.bios.2021.113737.

Rossetti, M., Srisomwat, C., Urban, M., Rosati, G., Maroli, G., Yaman Akbay, H.G., Chailapakul, O., Merkoçi, A., 2024. Unleashing inkjet-printed nanostructured electrodes and battery-free potentiostat for the DNA-based multiplexed detection of SARS-CoV-2 genes. Biosens. Bioelectron. 250, 116079 https://doi.org/10.1016/j.bios.2024.116079.

Sajedi-Moghaddam, A., Rahmanian, E., Naseri, N., 2020. Inkjet-printing technology for supercapacitor application: current state and perspectives. ACS Appl. Mater. Interfaces 12, 34487–34504. https://doi.org/10.1021/acsami.0c07689.

Salehi-Khojin, A., Estrada, D., Lin, K.Y., Ran, K., Haasch, R.T., Zuo, J.-M., Pop, E., Masel, R.I., 2012. Chemical sensors based on randomly stacked graphene flakes. Appl. Phys. Lett. 100, 033111 https://doi.org/10.1063/1.3676276.

Secor, E.B., Ahn, B.Y., Gao, T.Z., Lewis, J.A., Hersam, M.C., 2015. Rapid and versatile photonic annealing of graphene inks for flexible printed electronics. Adv. Mater. 27, 6683–6688. https://doi.org/10.1002/adma.201502866.

Secor, E.B., Prabhumirashi, P.L., Puntambekar, K., Geier, M.L., Hersam, M.C., 2013. Inkjet printing of high conductivity, flexible graphene patterns. J. Phys. Chem. Lett. 4, 1347–1351. https://doi.org/10.1021/jz400644c.

Šedajová, V., Bakandritsos, A., Błoński, P., Medveď, M., Langer, R., Zaoralová, D., Ugolotti, J., Dzíbelová, J., Jakubec, P., Kupka, V., Otyepka, M., 2022. Nitrogen doped graphene with diamond-like bonds achieves unprecedented energy density at high power in a symmetric sustainable supercapacitor. Energy Environ. Sci. 15, 740–748. https://doi.org/10.1039/D1EE02234B.

Shao, Y., Fu, J.-H., Cao, Z., Song, K., Sun, R., Wan, Y., Shamim, A., Cavallo, L., Han, Y., Kaner, R.B., Tung, V.C., 2020. 3D crumpled ultrathin 1T MoS_2 for inkjet printing of Mg-ion asymmetric micro-supercapacitors. ACS Nano 14, 7308–7318. https://doi.org/10.1021/acsnano.0c02585.

Silvestri, A., Vázquez-Díaz, S., Misia, G., Poletti, F., López-Domene, R., Pavlov, V., Zanardi, C., Cortajarena, A.L., Prato, M., 2023. An electroactive and self-assembling bio-ink, based on protein-stabilized nanoclusters and graphene, for the manufacture of fully inkjet-printed paper-based analytical devices. Small, 2300163. https://doi.org/10.1002/smll.202300163.

Sliz, R., Czajkowski, J., Fabritius, T., 2020. Taming the coffee ring effect: enhanced thermal control as a method for thin-film nanopatterning. Langmuir 36, 9562–9570. https://doi.org/10.1021/acs.langmuir.0c01560.

Soleymani, L., Li, F., 2017. Mechanistic challenges and advantages of biosensor miniaturization into the nanoscale. ACS Sens. 2, 458–467. https://doi.org/10.1021/acssensors.7b00069.

Suresh, R.R., Lakshmanakumar, M., Arockia Jayalatha, J.B.B., Rajan, K.S., Sethuraman, S., Krishnan, U.M., Rayappan, J.B.B., 2021. Fabrication of screen-printed electrodes: opportunities and challenges. J. Mater. Sci. 56, 8951–9006. https://doi.org/10.1007/s10853-020-05499-1.

Torrisi, F., Hasan, T., Wu, W., Sun, Z., Lombardo, A., Kulmala, T.S., Hsieh, G.-W., Jung, S., Bonaccorso, F., Paul, P.J., Chu, D., Ferrari, A.C., 2012. Inkjet-printed graphene electronics. ACS Nano 6, 2992–3006. https://doi.org/10.1021/nn2044609.

Urban, M., Rosati, G., Maroli, G., Pelle, F.D., Bonini, A., Sajti, L., Fedel, M., Merkoçi, A., 2023. Nanostructure tuning of gold nanoparticles films via click sintering. Small, 2306167. https://doi.org/10.1002/smll.202306167.

Urbanová, V., Holá, K., Bourlinos, A.B., Čépe, K., Ambrosi, A., Loo, A.H., Pumera, M., Karlický, F., Otyepka, M., Zbořil, R., 2015. Thiofluorographene–hydrophilic graphene derivative with semiconducting and genosensing properties. Adv. Mater. 27, 2305–2310. https://doi.org/10.1002/adma.201500094.

Vermisoglou, E., Panáček, D., Jayaramulu, K., Pykal, M., Frébort, I., Kolář, M., Hajdúch, M., Zbořil, R., Otyepka, M., 2020. Human virus detection with graphene-based materials. Biosens. Bioelectron. 166, 112436 https://doi.org/10.1016/j.bios.2020.112436.

Wu, J., Liu, H., Chen, W., Ma, B., Ju, H., 2023. Device integration of electrochemical biosensors. Nat. Rev. Bioeng. 1, 346–360. https://doi.org/10.1038/s44222-023-00032-w.

Xuan, T., Shi, S., Wang, L., Kuo, H.-C., Xie, R.-J., 2020. Inkjet-printed quantum dot color conversion films for high-resolution and full-color micro light-emitting diode displays. J. Phys. Chem. Lett. 11, 5184–5191. https://doi.org/10.1021/acs.jpclett.0c01451.

Xuan, X., Pérez-Ràfols, C., Chen, C., Cuartero, M., Crespo, G.A., 2021. Lactate biosensing for reliable on-body sweat analysis. ACS Sens. 6, 2763–2771. https://doi.org/10.1021/acssensors.1c01009.

Yakoh, A., Pimpitak, U., Rengpipat, S., Hirankarn, N., Chailapakul, O., Chaiyo, S., 2021. Paper-based electrochemical biosensor for diagnosing COVID-19: detection of SARS-CoV-2 antibodies and antigen. Biosens. Bioelectron. 176, 112912 https://doi.org/10.1016/j.bios.2020.112912.

Yang, Q., Nguyen, E.P., Panáček, D., Šedajová, V., Hrubý, V., Rosati, G., Silva, C. de C.C., Bakandritsos, A., Otyepka, M., Merkoçi, A., 2023. Metal-free cysteamine-functionalized graphene alleviates mutual interferences in heavy metal electrochemical detection. Green Chem. 25, 1647–1657. https://doi.org/10.1039/D2GC02978B.

Yun, C., Hwang, S., 2021. Analysis of the charging current in cyclic voltammetry and supercapacitor's galvanostatic charging profile based on a constant-phase element. ACS Omega 6, 367–373. https://doi.org/10.1021/acsomega.0c04702.

Zhao, H., Liu, F., Xie, W., Zhou, T.-C., OuYang, J., Jin, L., Li, H., Zhao, C.-Y., Zhang, L., Wei, J., Zhang, Y.-P., Li, C.-P., 2021. Ultrasensitive supersandwich-type electrochemical sensor for SARS-CoV-2 from the infected COVID-19 patients using a smartphone. Sensor. Actuator. B Chem. 327, 128899 https://doi.org/10.1016/j.snb.2020.128899.

Zhao, L., Rosati, G., Piper, A., de Carvalho Castro e Silva, C., Hu, L., Yang, Q., Della Pelle, F., Alvarez-Diduk, R.R., Merkoçi, A., 2023. Laser reduced graphene oxide electrode for pathogenic *Escherichia coli* detection. ACS Appl. Mater. Interfaces acsami.2c20859. https://doi.org/10.1021/acsami.2c20859.

Zub, K., Hoeppener, S., Schubert, U.S., 2022. Inkjet printing and 3D printing strategies for biosensing, analytical, and diagnostic applications. Adv. Mater. 34, 2105015 https://doi.org/10.1002/adma.202105015.